CHEMISTRY
A European Journal

A Journal of
ChemPubSoc Europe

Accepted Article

Title: Rationally Designed Blue Triplet Emitting Gold(IIII) Complexes Based on Phenylpyridine Derived Framework

Authors: Michael Bachmann, Jasmin Terreni, Olivier Blacque, and Koushik Venkatesan

To be cited as: *Chem. Eur. J.* 10.1002/chem.201605567

Link to VoR: http://dx.doi.org/10.1002/chem.201605567

Supported by
ACES

WILEY-VCH

10.1002/chem.201605567

WILEY-VCH

Rationally Designed Blue Triplet Emitting Gold(III) Complexes Based on Phenylpyridine Derived Framework

*Michael Bachmann, Jasmin Terreni, Olivier Blacque, and Koushik Venkatesan**[a]

Department of Chemistry, University of Zurich, Winterthurerstrasse 190, CH-8057 Zurich, Switzerland

Abstract: A series of blue emitting phosphorescent monocyclometalated Au(III) complexes were successfully synthesized. Tailoring substitutions at the phenylpyridine (ppy) ligand scaffold with the electron withdrawing fluorine groups at the phenyl ring to achieve stabilization of the HOMO and electron donating dimethylamino group on the pyridine ring to destabilize the LUMO resulted in a large energy gap and bestowed the gold(III) complexes with emission at high energies and high quantum efficiencies. Cyclic voltammetry (CV) studies are suggestive of a predominantly cyclometalated ligand localized redox event. Thermogravimetric analysis (TGA) of selected complex displayed a high stability up to 280 °C, making the complexes suitable for device fabrication through vacuum deposition. Photophysical investigations performed for all the derivatives displayed phosphorescence emission in neat solid, solution, doped in poly(methyl methacrylate) (PMMA) films at room temperature as well as in rigidified glass media (2-MeTHF) at 77 K. A high photoluminescent quantum efficiency up to 28% was obtained for a complex in PMMA, the highest quantum yield reported for a blue emitting gold(III) complex.

Introduction

Investigation of tunable room temperature phosphorescent metal complexes have gained a widespread interest in the last decennaries following the near-commercialization of cyclometalated iridium(III) and platinum(II) complexes for applications in OLEDs (organic light emitting diode).[1a-e] While gold(I) complexes have intensively been studied in their photochemical properties[1f,1g] and have shown to be active in photoredox catalysis recently[1h,1i], gold(III) complexes remain underexplored for their luminescent properties in comparison to the isoelectronic platinum(II) and iridium(III) counterparts which can be ascribed to a number of reasons.[2] These reasons mostly include the moderate stability of organogold(III) compounds and the low-lying d-d ligand field (LF) states of gold(III) complexes, with the latter one known to deactivate excited-states non-radiatively. On the contrary, the spin-orbit coupling constant of gold (ζ = 5100 cm^{-1}) is even higher than those of platinum or iridium, which is beneficial for the radiative decay of the triplet excited states.[3] In recent past, more attention in exploration of the basic photophysical properties of Au(III) complexes has gained increased exploration for applications as efficient small molecule phosphors in OLED devices.[4]

To overcome the aforementioned disadvantages, a successful strategy was pursued by the group of Yam that involved the use of strong field ligands with good σ-donating properties as ancillary ligands in order to decrease the probability for thermal population of non-emissive d–d states.[5] Utilizing such an approach, Yam reported the first luminescent gold(III) complexes in 1990 and later followed it by the development of room temperature luminescent biscyclometalated gold(III) complexes.[6] The tridentate ligand system has been further exploited by other groups to access new luminescent gold(III) complexes.[7] Based on the initial impetus and subsequent studies, our group had recently demonstrated phenyl pyridine (*ppy)* based mono-cyclometalating ligands as a promising framework for obtaining stable, luminescent gold(III) complexes.[8] Since phenyl is a better σ-donating ligand than pyridine, the introduction of a cyclometalating *ppy* instead of the bipyridine (*bipy)* was assumed to further increase the energy level of the d-d-states. In addition to the cyclometalation, employment of strong field aromatic stabilized carbanions as ancillary ligands was expected to sufficiently destabilize the metal centered (MC) transition to higher energies thereby creating a conducive metal-ligand environment for effective mixing of singlet-triplet states and radiative relaxation from the triplet manifold. Adopting such a strategy yielded stable complexes with long-lived emission in solution at room temperature and tunable emission energies with λ_{max} centered from 490 nm to 590 nm depending on the electronic character of the arylpyridine derivative. Although access to green and red emitting complexes could be successfully achieved, gold(III) complexes based photoactive materials displaying emission in the blue / deep blue region of electromagnetic spectrum is lacking. One of the main problem currently being faced is the production of high-quality blue-emitting OLEDs in general.[9] There are three challenges that have to be overcome concerning the development of efficient blue triplet emitters. Firstly, the chromaticity of the most available blue phosphor is not a true blue color (λ_{max} 435 nm), which gives a poorer color spectrum for applications in full color OLED displays. Secondly, the emission quantum efficiency of blue phosphors is far lower than green and red phosphors, which has significant consequences on the quality of the white light, especially in the case of cold white light, which requires a larger share of the blue part of the electromagnetic spectrum. Finally, the working

[a] M. Bachmann, J. Terreni, Dr. O. Blacque, Dr. K. Venkatesan
Department of Chemistry
University of Zurich
Winterthurerstrasse 190
CH-8057, Zurich (Switzerland)
Fax: (+41)446356803
E-mail: venkatesan.koushik@chem.uzh.ch

Supporting information for this article is given via a link at the end of the document.((Please delete this text if not appropriate))

lifetime of most of the blue dyes in OLEDs are often thousands of hours shorter than those of green and red counterparts, which is a property relevant to their phosphorescence efficiency and is influenced by their molecular tailoring and device construction. The reason for the relatively faster degradation of the blue dyes can be attributed to the requirement of higher excitation energy. The higher in energy an excited state is situated, the more likely it is that a reactive potential lies in between this and the ground state. In short, the emissive substance is more likely to decompose.[10] The poor stability of blue phosphors unfortunately makes such displays visually much faster distorted than would be acceptable for a commercially viable device. Therefore, investigations pertaining to efficient and stable blue triplet emitters are of high demand in order to drastically improve the performance of the OLED devices and are crucial for its commercial application. Although, a Au(III) blue emitting phosphor is known based on a tridentate biscyclometalated system, it possesses only a weak emission.[11a] Initial studies in our group on the unsubstituted *ppy* Au(III) complexes showed the origin of the emission to arise from an intraligand charge transfer (^{3}ILCT) [π-π*] perturbed by the metal center. This was further confirmed by DFT and TD-DFT calculations that revealed the HOMO to be almost entirely localized on the phenyl part of the cyclometalated ligand and the LUMO at the pyridine moiety due to the better accepting properties. Based on the above information, we approached to rationally alter the ligand scaffold of the monocyclometalated gold(III) complexes[11b] to achieve the desired blue emission.[8a] As illustrated in Scheme 1, addition of electron withdrawing substituents such as F, CF_3 and OCF_3 on the phenyl group was expected to result in a decreased energy level of the HOMO and substitution of the pyridine with an electron donating group such as dimethylamine increasing the corresponding LUMO state, respectively.

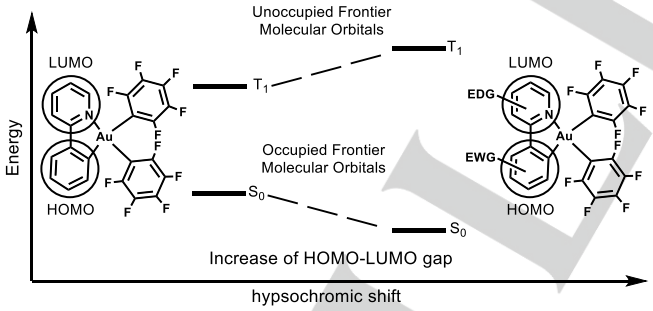

Scheme 1. Concept of hypsochromic shift caused by increase of HOMO-LUMO gap.

Besides, fluorinated compounds also bring along several advantages. The increased electronegativity of the ligands profits in a better overlap towards the low-lying Au(III) orbitals and therefore resulting in a higher stability of the final compounds. The bulky substituents, such as CF_3 or OCF_3 hinder the stacking of the compounds and can possibly inhibit self-quenching effects and further, the sublimation for thin film deposition is enhanced.[12] Based on the above concepts, we deemed it possible to achieve efficient blue triplet emitters and additionally also obtain a closer insight into the effects of the different substitutions of the C^N cyclometalated ligands on the photoluminescent properties of the corresponding Au(III) complexes, which remains rather underdeveloped.

Results and Discussion

Synthesis and characterization

Compounds **1**–**4** were synthesized as colorless solids in 39–62% yield starting from the different cyclometalated *cis*(N^C)$AuCl_2$ derivatives and subsequent substitution of the chlorides with pentafluorophenyl ligand in the case of complexes **1**, **3**, **4** and ethynyl-4-fluorophenyl for complex **2** according to the synthetic strategy shown in Scheme 2. All the final compounds were characterized by ^{1}H, ^{13}C, ^{19}F NMR and elemental analysis. The successful coordination of the pyridine derivatives to the mercury center could be verified due to the absence of the proton resonance in the ^{1}H NMR spectra with the other proton resonances showing any significant shift. The later transmetallation step in order to obtain the corresponding gold precursor, showed a distinct downfield shift of around 0.6–0.8 ppm from the α proton on the pyridine due to the deshielding of the proton after coordination to the nitrogen. In the final products, ^{19}F NMR measurements revealed the efficacious bonded ancillary aryl or alkyne ligands. As expected the spectra showed additional six different resonances for the two pentafluorophenyls and two signals for the 4-fluorophenylacetylene, respectively, which is in good agreement with the two unequal *trans* standing ligands to the cyclometalating moiety. Due to the absence of NOE effect, overlap of signals and coupling with different fluorine atoms, only undefined small multiplets were observed for the carbon signals of the pentafluorophenyl ligand in the ^{13}C NMR.

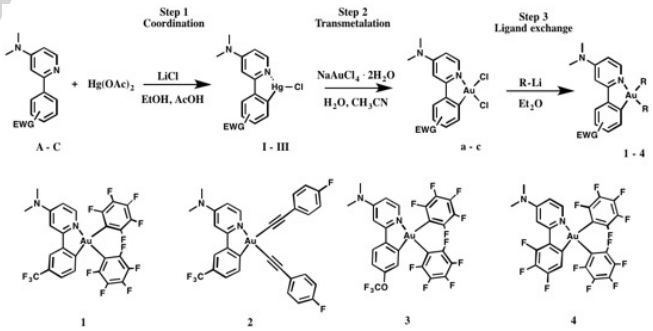

Scheme 2. Synthetic pathway for complexes **1**–**4.**

In addition, the crystal structure of complex **4** was determined by an X-ray diffraction study (Figure 1) on suitable single crystals, which were obtained by slow diffusion of hexane into a dichloromethane (CH_2Cl_2) solution containing a small concentration of the compound. Crystallographic data and selected bond distances and angles are given in Table 1 (further data are given in Supporting Information). The Au(III) complex possesses a square planar geometry. The cyclometalated ligand

is almost planar with the angle between the mean planes of the phenyl and pyridine rings of the cyclometalated ligand only being 1.44(12)°. The methyl substituents of the dimethylamino group are coplanar with the pyridine ring and the corresponding carbon atoms deviate from the mean plane by only 0.043(3) and 0.158(3) Å. The pentafluorophenyl ligands lie almost perpendicular to the phenylpyridine. The angles between the mean planes of the C_6F_5 rings and the pyridine ring are 71.96(13) and 71.74(13)°. The Au–C bond length between the metal center and the pentafluorophenyl ligand is slightly shorter in the case of the ligand *trans* to the pyridine nitrogen atom than in the case of the ligand *trans* to the 2,3,4-fluorophenyl part (2.014(2) *vs.* 2.080(3) Å) which is in a good agreement with the stronger *trans* influence of phenyl *vs.* pyridine ligand in general. The crystal packing of the structure exhibits some C–H···F and C–F···π intermolecular interactions, the shortest H···F and F···centroid contacts are 2.57 and 3.065(2) Å, respectively, but no π···π or Au···Au interactions (the shortest Au···Au distance is 5.4210(3) Å) were observed.

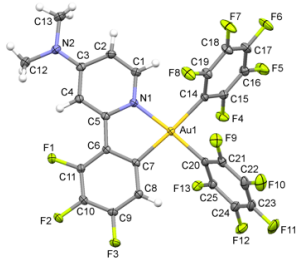

Figure 1. X-ray crystal structure of **4** with selective atomic numbering scheme. Thermal displacement ellipsoids are drawn at the 30% probability level.

These complexes were found to have overall the same thermal stability. Thermogravimetric analysis (TGA) of complex **1** displayed an onset of total degradation at 280 °C (Figure S1). Such high thermal stability makes these classes of complexes suitable for OLED device fabrication through vacuum deposition

Table 1. Selected bond distances (Å) and angles (°) for complex **4**.

Au1-N1	2.054(2)
Au1-C7	2.048(3)
Au1-C20	2.014(2)
Au1-C14	2.080(3)
N1-Au1-C14	95.84(9)
C7-Au1-N1	80.46(9)
C7-Au1-C14	176.29(9)
C20-Au1-N1	175.74(9)
C20-Au1-C7	95.34(10)
C20-Au1-C14	88.37(10)

Photophysical properties

The UV/Vis absorption spectra of **1**–**4** in CH_2Cl_2 at 298 K are shown in Figure 2. All four complexes exhibit two strong bands at wavelengths below 300 nm and a moderate intense band at 310–360 nm. Based on the spectroscopic studies, the absorption bands are mainly assigned to origin of an admixture of metal-perturbed ^{1}ILCT. Concentration dependent absorption studies of all the complexes in CH_2Cl_2 ($c \approx 10^{-6}$–10^{-4} mol dm^{-3}) displayed no development of an additional low energy band or shifting in the λ_{max} supporting the absence of any aurophilic interactions in solution and precluding excimeric metal to metal charge transfer (^{3}MMLCT) transitions. Varying the ancillary ligands on the cyclometalated gold center had no distinct effect on the absorption wavelengths except only a small bathochromic shift of the high energy absorption band was observed which is due to the increased electron density at the phenylacetylene compared to the pentafluorophenyl counterpart.

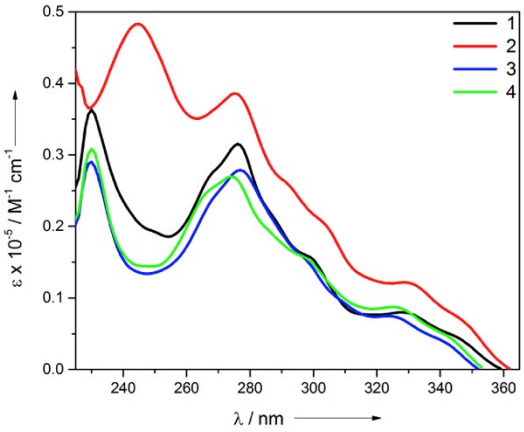

Figure 2. UV/Vis absorption spectra of complexes **1**–**4** in CH_2Cl_2.

Increasing solvent polarity from cyclohexane to acetonitrile leads only to a small hypsochromic shift (λ ~ 10 nm) for complex **1** indicating the ground state has more polar constitution as compared to the excited state (Figure S2). Complexes **1**–**4** exhibit strong emission in fluid solution at room temperature, doped in PMMA and in rigidified glass media (2-MeTHF) at 77 K. The spectroscopic data for complexes **1**–**4** are given in Table 3 and the emission profiles in different media for all the complexes are shown in Figure 3–5. The emission wavelengths were not significantly influenced by their different electron withdrawing groups and further didn't display remarkable shifts between solution and PMMA films except for complex **4** which showed a much broader and less structured emission band in fluid solution at room temperature compared to the other derivatives. To verify that no excimeric states were formed, additional concentration dependent measurements were performed. The outstretched emission profile didn't change after dilution in CH_2Cl_2, declined in toluene and disappeared completely in THF indicating the fact that this behavior is ascribed to the inherent nature of this

compound and is not induced by intermolecular interactions (Figure 6). Further investigations in the future are required to ascertain the origin of this behavior. Supplementary measurements such as excitation spectra and concentration dependence of the PMMA films can be found in the supporting information (Figure S3, S4). A small bathochromic shift of the emission wavelength was observed while increasing the doped wt% of complex **1** from 2% to 30%, which can be attributed to minor intermolecular quenching effects.

On the basis of the above observations and previous studies on the unsubstituted *ppy* derivatives in our group, the origin of the emission is assigned to arise from an intraligand charge transfer (ILCT) [π-π*] perturbed by the metal center. Stokes shifts and lifetimes in the lower microsecond range strongly imply that the emission takes place from the triplet state. DFT and TD-DFT calculations (For a detailed discussion, see later section on DFT and TD-DFT calculations) on *ppy* Au(III) complexes further underscores our presumption that the corresponding admixtures of the HOMO's is almost entirely localized on the phenyl part of the cyclometalated ligand and the LUMO's at the pyridine moiety due to the favorable accepting properties. As hypothesized inclusion of an electron withdrawing substituent at the phenyl decreased the energy level of the respective HOMO's and substitution at the pyridine with the electron donating NMe_2 increases the levels of the LUMO's, respectively. Overall the emission showed hypsochromic shifts with highest energy emission maxima in the range λ_{max} = 420–438 nm. This corresponds to a blue shift of up to 27 nm in comparison to the parent phenylpyridine analogue.

Figure 7 shows representative 1931 Commission Internationale de L'Eclairage coordinates (CIE *x*,*y*) calculated from the photoluminescence spectrum in PMMA and the corresponding values are listed in Table 2. For example, devices using the nowadays leading FIrpic dopant as the chromophore usually exhibit CIE coordinates around (0.18,0.33).[13] The CIE coordinates of these complexes, which remain in the dimension up to (0.15,0.13) are much closer to the desired true-blue color (0.14,0.08).

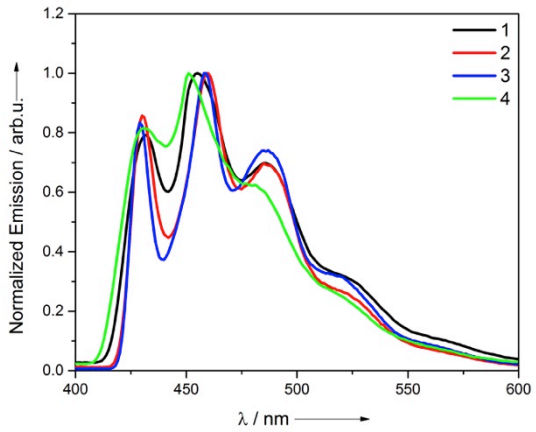

Figure 3. Emission spectra of complexes **1**–**4** in 2-MeTHF at 77 K.

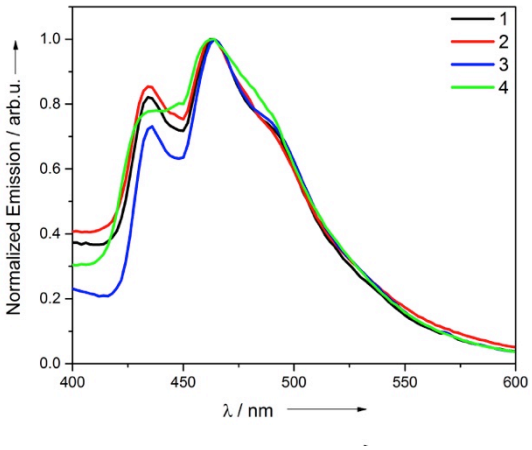

Figure 4. Emission spectra of complexes **1**–**4** in 2wt% in PMMA films.

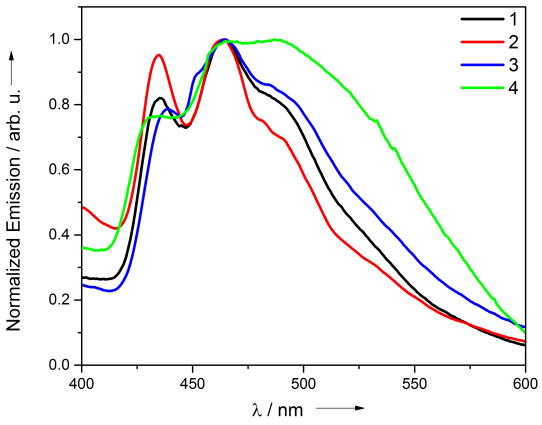

Figure 5. Emission spectra of complexes **1**–**4** in solution.

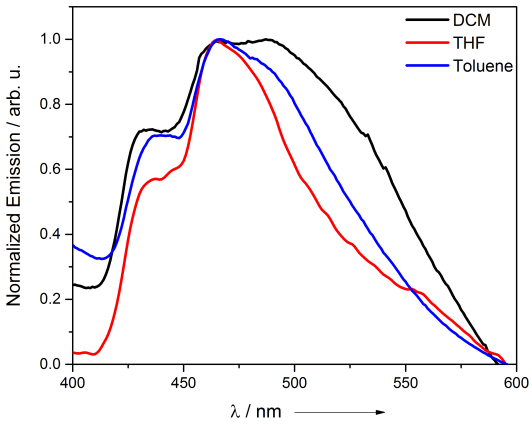

Figure 6. Normalized emission spectra of **4** in different solvents.

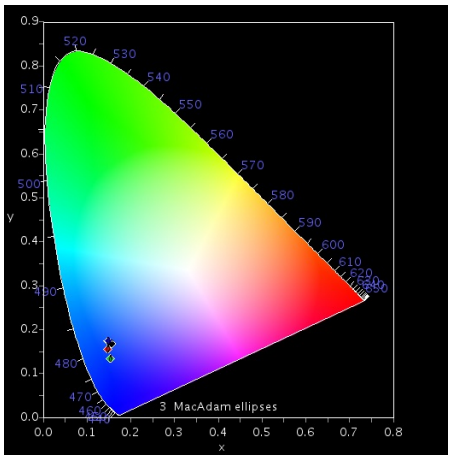

Figure 7. CIE-1931 diagram of **1**–**4** in 2wt% in PMMA films.

Table 2: Emission coordinates of **1**–**4** on the CIE-1931 chromaticity diagram.

Complex	X / Y
1	0.1565 / 0.1679
2	0.1480 / 0.1557
3	0.1488 / 0.1737
4	0.1540 / 0.1341

Table 3. Photophysical properties of complexes **1**–**4**.

	Absorption (CH_2Cl_2)		Emission			
Complex	λ_{max}/nm (ε /$M^{-1}cm^{-1}$)	Medium (T/K)	λ_{max}/nm (τ_0/ µs)	ϕ_{em} (%)	k_r [×$10^3 s^{-1}$]	k_{nr} [×$10^5 s^{-1}$]
1	230 (36655) 276 (31525) 331 (7715)	glass (77) PMMA (298) DCM (298)	431, 455, 486, 527 sh 435, 463, 489 sh (1.15) 435, 464, 489 sh	- 28.1	243.5	6.3
2	275 (38596) 330 (12117)	glass (77) PMMA (298) DCM (298)	430, 459, 486, 525 sh 435, 462 (0.18) 435, 464, 490 sh	- 3.0	166.7	53.9
3	230 (30820) 277 (27866) 324 (7487)	glass (77) PMMA(298) DCM (298)	429, 458, 487, 521 sh 436, 464, 491 sh (2.09) 439, 464, 495 sh	- 4.5	21.5	4.5
4	230 (30820) 274 (26981) 324 (8745)	glass (77) PMMA (298) DCM (298)	431, 451, 481, 524 sh 434, 463 (3.21) 436, 465, 487	- 27.6	86.3	2.3

Electrochemical properties

Cyclic voltammetry investigations of all four complexes displayed irreversible reduction peaks in the range of -2.04 to -2.40 V (vs $Fc^{0/+}$ couple) in DMF at room temperature (Table 4). No oxidation peak was observed. Considering the congruence of the reduction peak potentials among the diverse compounds, the reduction event is referred to be a predominately ligand centered electrochemical process.

Table 4. Electrochemical potentials for complexes **1–4** in 0.1 M [nBu_4N][PF_6] (glassy-carbon electrode; E vs $Fc^{0/+}$; scan rate = 100 mV/s; 20°C, DMF).

Complex	Reduction E_{pc}/V vs $Fc^{0/+}$
1	-2.04
2	-2.13
3	-2.11
4	-2.40

DFT and TD-DFT calculations

TD-DFT calculations were carried out on the DFT optimized ground state geometry of complexes **1**–**4** (see Computational Details and Supporting Information). In the case of **1**, **3** and **4**, they clearly confirm the spectroscopic evidences that the three moderate to intense absorption bands experimentally observed predominantly arise from an intraligand charge transfer ^{1}ILCT within the cyclometalated N^C ligand. The most important contributions to the calculated π→ π* transitions come from the HOMO→LUMO, HOMO-1→LUMO, and HOMO→LUMO+2 excitations involving four frontiers molecular orbitals mainly localized on the N^C ligand and the metal center (Figure 8, Figures S9, S11-S13, S16, S17). It is slightly different for the alkyne containing complex **2**. The first two singlet-singlet S_0-S_1 and S_0-S_2 transitions for **2** (331.6 and 325.0 nm, oscillator strengths *f* = 0.139 and 0.441, respectively) resulting into a moderate intense absorption band, are ligand-to-ligand ^{1}LLCT transitions coming from the HOMO→LUMO and HOMO-

1→LUMO excitations: the occupied frontier orbitals being mainly located on the alkyne ligands (and on the dimethylaminopyridine ligand for HOMO-1) and the unoccupied orbital on the cyclometalated ligand. The two other bands in the 240 – 280 nm region correspond to a mixing of $^1ILCT_{(N^C)}$, $^1ILCT_{(alk)}$ and $^1LLCT_{(alk\rightarrow N^C)}$ transitions. Nevertheless, the geometry optimization of complex **2** suggested that the C≡C-(C_6H_4F) alkyne ligands are relatively free to rotate around the Au – C bond. The fully optimized geometry (without constraint) of complex **2** exhibits a relatively planar conformation characterized by the two torsional angles N1-Au1-C1-C2 and C3-Au1-C4-C5 of 25.1 and -4.7°, respectively (Figure S10). A relaxed potential energy surface scan (with geometry optimization at each point) was performed with two variables as the previously defined torsional angles X-Au-C-C (X = N or C). The two variables were varied together from 0 to 90° (step of 15°) to reach a final conformation for which the terminal C_6H_4F benzene rings are perpendicular to the (N^C) plane. The latter conformation will be noted **2B** in the manuscript, while the fully optimized structure will be **2** or **2A**. The calculations revealed that **2B** is only 0.25 kcal/mol higher in energy than **2A** without energy barrier on the way indicating a free rotation of the alkyne ligands in solution at room temperature, experimental conditions of the UV/Vis studies. TD-DFT calculations as single point calculations on all studied conformations of **2** show that the ^1LLCT absorption band formed by the two S_0-S_1 and S_0-S_2 transitions of **2A** decreases in intensity with the rotation of the C_6H_4F groups from almost coplanar to perpendicular (**2B**) to the cyclometalated ligand (Figure S14, S22). The oscillator strength of the S_0-S_1 and S_0-S_2 transitions decrease and the first significant transition becomes S_0-S_3 (312.7 nm, f = 0.249), a $^1ILCT_{(N^C)}$ transition arising from the HOMO-2→LUMO excitation. The two strong bands at wavelengths below 300 nm remain from mixed origins but are calculated to be shifted closer to each other.

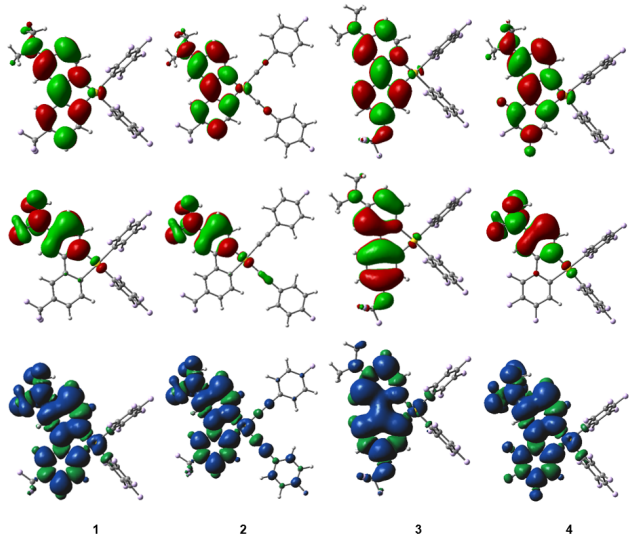

Figure 8.
Singly occupied molecular orbitals (top:SOMO, middle: SOMO-1) obtained by restricted open-shell single pointcalculations on the optimized triplet state geometries, and spin densitysurfaces (bottom) for the optimized triplet states of **1**–**4** (the positive spin densities are shown in blue and the negative ones are in green).

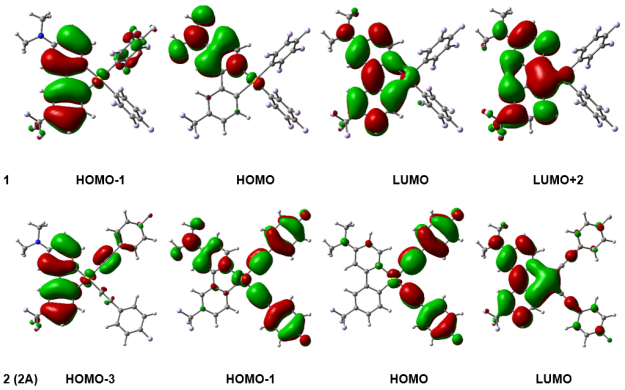

Figure 9. Spatial plots of selected frontier orbitals of the DFT optimized ground state of **1** and **2** (2A).

Table 5. Selected singlet (S_1, and S_n with oscillator strength $f > 0.1$) and triplet T_m excited states (m = 1-3) calculated with TD-DFT/CPCM (in dichloromethane): vertical excitation energies (nm), transition coefficients ($c > 0.2$), orbitals involved in the transitions, and oscillator strengths f for compounds **1**–**4**. * H = HOMO, L = LUMO

	1	**2A**	**2B**	**3**	**4**
S_0–S_n	n = 1	n = 1	n = 1	n = 1	n = 1
	309.6 (f = 0.170)	331.6 (f = 0.139)	331.5 (f = 0.000)	303.5 (f = 0.223)	306.0 (f = 0.195)
	H→L (c = 0.68) [a]	H→L (c = 0.69)	H→L (c = 0.69)	H→L (c = 0.67)	H→L (c = 0.69)
	n = 2	n = 2	n = 3	n = 3	n = 2
	283.2 (0.166)	325.0 (0.441)	312.7 (0.249)	290.3 (0.256)	284.8 (0.224)
	H-1→L (0.65)	H-1→L (0.69)	H-2→L (0.69)	H-1→L (0.68)	H-1→L (0.66)
	n = 5	n = 6	n = 4	n = 6	n = 1
	265.2 (0.160)	279.4 (0.308)	290.0 (0.154)	261.6 (0.318)	258.3 (0.592)
	H→L+2 (0.40)	H→L+1 (0.59)	H-3→L (0.67)	H→L+2 (0.48)	H→L+2 (0.59)
	H-6→L (0.38)			H-4→L (0.24)	
				H-2→L (0.20)	
	n = 6	n = 7	n = 5	n = 7	n = 1
	264.0 (0.356)	276.2 (0.365)	276.4 (0.239)	260.7 (0.158)	235.2 (0.220)
	H→L+2 (0.46)	H-1→L+1 (0.63)	H→L+2 (0.65)	H-3→L+1 (0.28)	H-1→L+2 (0.65)
				H→L+2 (0.25)	
	n = 9	n = 13	n = 7	n = 8	
	260.0 (0.104)	258.1 (0.228)	273.1 (0.155)	259.1 (0.309)	
	H-4→L (0.31)	H-2→L+1 (0.37)	H-1→L+2 (0.62)	H→L+2 (0.33)	
	H-1→L+1 (0.26)	H→L+6 (0.32)	H-1→L+7 (0.20)	H-5→L+1 (0.30)	
	H-5→L+1 (0.21)	H→L+ (0.22)		H-4→L+1 (0.22)	
	n = 15	n = 14	n = 8	n = 15	
	237.9 (0.288)	257.6 (0.196)	271.1 (0.155)	244.1 (0.152)	
	H→L+3 (0.48)	H-2→L+1 (0.33)	H-4→L (0.43)	H-1→L+2 (0.52)	
			H-3→L+1 (0.25)	H-6→L (0.39)	
	n = 16	n = 16	n = 10		
	236.7 (0.115)	250.1 (0.273)	265.9 (0.422)		
	H→L+3 (0.44)	H→L+4 (0.41)	H-2→L+1 (0.63)		
	H-1→L+2 (0.36)	H-1→L+2 (0.36)			
		H→L+3 (0.22)			
		n = 17	n = 11		
		247.9 (0.177)	261.8 (0.184)		
		H-1→L+2 (0.37)	H-4→L (0.51)		
		H-1→L+4 (0.22)	H-5→L (0.45)		
			n = 15		
			255.1 (0.660)		
			H→L+3 (0.63)		
			n = 17		
			247.9 (0.110)		
			H-3→L+1 (0.38)		
			H-5→L (0.30)		
			H-1→L+3 (0.23)		
			n = 19		
			245.1 (0.466)		
			H-1→L+3 (0.55)		
S_0–T_1	413.0	419.6	416.1	418.7	408.2
	H-1→L (0.59)	H→L (0.29)	H-3→L (0.56)	H-1→L (0.61)	H-1→L (0.61)
	H-6→L+2 (0.20)				
S_0–T_2	389.2	414.4	405.2	381.0	391.5
	H→L (0.66)	H-1→L (0.30)	H-1→L+2 (0.36)	H→L (0.65)	H→L (0.66)
			H→L+2 (0.35)		
			H-7→L+5 (0.20)		
S_0–T_3	330.6	408.7	400.9	328.3	327.7
	H→L+2 (0.53)	H-3→L (0.36)	H→L+3 (0.43)	H→L+2 (0.58)	H→L+2 (0.61)
			H-6→L+6 (0.21)		

The emission spectra recorded in dichloromethane at room temperature indicated similar luminescent properties for all complexes with maximum emission wavelengths in the narrow range of 435 – 439 nm. The lowest singlet-triplet T_1–S_0 energies obtained from the ground state structures of **1**–**4** are in a good agreement with the experimental data (Table 5). Indeed, the calculated energy values are very close to each other, in the range 408 – 418 nm, underestimating the experimental data by about 20 nm only. The first triplet excited state T_1 of **1**, **3** and **4** originates from the HOMO-1→LUMO excitation. The S_0-T_1 transition can be assigned as an intraligand charge transfer ^{3}ILCT between π and π* orbitals of the cyclometalated ligand N^C. Taking into account the ground state geometry of **2** (**2A**), the first triplet excited state T_1 originates from the HOMO→LUMO excitation and the corresponding S_0-T_1 transition (419.6 nm) can be assigned as a ligand-to-ligand charge transfer ^{3}LLCT$_{(alk→N^C)}$ between π orbitals of the alkynes ligands and π* orbitals of the cyclometalated ligand. The ^{3}ILCT$_{(N^C)}$ triplet state is computed as T_3 (408.7 nm) while T_2 (414.4 nm) arises essentially from a ^{3}LLCT$_{(alk→N^C)}$ transition like the lowest triplet state T_1. The energy and character of the first three triplet excited states of complex **2** were also investigated in relation with the rotation of the terminal C_6H_4F groups of the alkyne ligands (Tables S1-S2). The study revealed that the ^{3}ILCT$_{(N^C)}$ triplet state, T_3 for the coplanar ground state geometry **2A**, becomes the emitting triplet state T_1 for the perpendicular conformation **2B**. In fact, T_1 exhibits mainly a ^{3}LLCT$_{(alk→N^C)}$ character as long as the dihedral angle variables remains in the interval 0 – 30° but that character rapidly vanishes to disappear from 45° (Figure S23). From that point, T_1 exclusively originates from a ^{3}ILCT$_{(N^C)}$ transition arising from the HOMO-3→LUMO excitation. The two other calculated lowest triplet excited states T_2 and T_3 come from mixed ^{3}LL and ^{3}IL transitions. The lowest triplet state structure of each complex was optimized by unrestricted calculations. The spin density surfaces and the singly occupied molecular orbitals obtained from restricted open shell calculations are displayed on Figure 9. The results confirm the ^{3}ILCT$_{(N^C)}$ origin of the emission but also highlight the role of the dimethylaminopyridine moiety in the luminescent process.

Conclusions

It is demonstrated through monocyclometalated compounds of the type *cis*-[(N^C)AuL$_2$] (L = aryl, alkyne) for the first time that true blue phosphorescent emission based on gold(III) complexes can be achieved with the highest efficiency reported so far. They display luminescence at room temperature in fluid solution and their emission wavelengths can be tuned by changing the substituents on the cyclometalating ligand. Of particular interest is complex **1** with the excellent quantum efficiency of 28% in PMMA and the high stability making them suitable for vacuum deposition for enabling OLED applications. DFT calculations in conjunction with experimental work have ascertained the relative stability of the complexes and the nature of the triplet excited state. The stability and ease of tunability of the blue emitting gold(III) complexes demonstrated in this work paves way for the development of new efficient blue gold(III) triplet emitting molecules and further strengthens their prospects for OLED applications.

Experimental Section

General procedure

All manipulations requiring inert atmosphere were carried out using standard Schlenk techniques under dinitrogen. ^{1}H, ^{13}C{^{1}H} and ^{19}F NMR spectra were recorded on Bruker 400 MHz and 500 MHz spectrometers. Chemical shifts (δ) are reported in parts per million (ppm) referenced to tetramethylsilane (δ 0.00) ppm using the residual proton solvent peaks as internal standards (^{1}H NMR experiments) or the characteristic resonances of the solvent nuclei (^{13}C NMR experiments). ^{19}F NMR was referenced to $CFCl_3$ (δ 0.00) ppm. Coupling constants (*J*) are quoted in Hertz (Hz) and the following abbreviations are used to describe the signal multiplicities: s (singlet); d (doublet); t (triplet); q (quartet); quint (quintet); sext (sextet); sept (septet); m (multiplet). Proton and carbon assignments have been made using routine one and two dimensional NMR spectroscopies where appropriate. Elemental microanalysis was carried out with Leco CHNS-932 analyzer. TLC analysis was performed on precoated Merck Silica Gel60F254 slides and visualized by luminescence quenching either at (short wavelength) 254 nm or (long wavelength) 365 nm. Chromatographic purification of products was performed on a short column (Length 30.0 cm; diameter 3.0 cm) using silica gel 60, 230–400 mesh using a forced flow of eluent. UV/Vis absorption measurements were carried out on a Perkin-Elmer Lambda 35 UV/Vis spectrophotometer. Emission spectra were acquired on Perkin Elmer spectrophotometer using 450 W Xenon lamp excitation by exciting at the longest-wavelength absorption maxima with the excitation slit width 5 nm and emission slit width 10 nm. Absolute quantum yields ϕ_{em} were determined at 298 K in thin films using an integrating sphere on the Edinburgh spectrophotometer FLS920 (estimated uncertainty ± 15 %). YAG:Ce (powder) was used as a calibration reference with ϕ_{em} = 97 %. Phosphorescent lifetimes in thin films were measured on the Edinburgh laser flash photolysis spectrophotometer LP920 with a Nd:YAG 355 nm laser as an excitation source fitted with a single monochromator. Photo excited emission color CIE-1931 chromaticity diagrams were determined using normalized emission spectra and the ColorCalculator Version 5.31 from Osram Sylvania. Cyclic voltammograms were measured with a Metrohm 757 VA Computrace with a glassy carbon electrode (d = 2mm) with a Pt counter electrode versus Ag/AgCl reference electrode.

All starting materials were purchased from commercial sources and used as received unless otherwise stated. All chemicals were of reagent grade and the solvents used for synthesis were of analytical grade.

2-bromo-4-(*N,N*-dimethylamino)pyridine

In a *Schlenk* flask containing dry hexane (40 mL) at –5°C, dimethylethanolamine (4.90 mL, 49 mmol) was added. 2.5 M *n*BuLi (39 mL, 97.5 mmol) was added and the reaction mixture was stirred for 1 h. Further, dimethylaminopyridine (2.95 g, 24.2 mmol) was added to give an orange mixture and this mixture was stirred at 0°C for 2 h. After, the reaction mixture was cooled to –80°C and tetrabromomethane (20.0 g, 60.4 mmol) dissolved in dry hexane was added to the reaction mixture. After stirring for 1 h, the reaction mixture was quenched with H_2O resulting in a complete black solution. The aqueous phase was extracted with Et_2O and the combined organic phases were dried over $MgSO_4$. Evaporation of the solvent *in vacuo* delivered the crude product. The crude product was purified by flash chromatography on silica gel (eluent: AcOEt) to give the title compound as an off-white solid. Yield = 2.56 g, 12.8 mmol, 61%. ^{1}H NMR (400 MHz, CD_2Cl_2, 25°C, TMS): δ=7.89 (d, ^3J(H,H)=6 Hz, 1H), 6.64 (d, ^4J(H,H)=2.5 Hz, 1H), 6.46 (dd, ^3J(H,H)=6 Hz; ^4J(H,H)=2.5 Hz, 1H), 2.97 ppm (s, 6H).

2-(3-trifluoromethylphenyl)-4-(*N,N*-dimethylamino)pyridine (A)

To a *Young Schlenk* flask, 2-bromo-4-(*N,N*-dimethylamino)-pyridine (1.00 g, 4.97 mmol), 3-trifluoromethylphenyl)boronic acid (1.13 g, 5.97 mmol) and NaOH pellets (477 mg, 12.0 mmol) were added. To this reaction mixture, H_2O (15 mL) and dioxane (25 mL) were added. After degassing the reaction mixture, $Pd(PPh_3)_4$ dissolved in THF (approx. 7 mL) was added to the reaction mixture, which was then heated to 100°C for 16 h. After the reaction mixture was allowed to cool to room temperature, the aqueous phase was extracted with CH_2Cl_2 and the organic phases were washed with H_2O. Drying of the combined organic phases with $MgSO_4$ and evaporation of the solvent *in vacuo* delivered the crude product. The crude product was further purified by flash chromatography on silica gel (eluent: CH_2Cl_2/AcOEt 1:1) to afford the title compound as an off-white solid. Yield = 770 mg, 2.89 mmol, 58%. ^{1}H NMR (400 MHz, CD_2Cl_2, 25°C, TMS): δ=8.29 (d, ^3J(H,H)=5.6 Hz, 1H), 8.27 (m, 1H), 8.18 (dd, ^3J(H,H)=7.7 Hz; ^4J(H,H)=1.1 Hz, 1H), 7.65 (m, 1 H), 7.58 (m, 1H), 6.96 (d, ^4J(H,H)=2.5 Hz, 1H), 6.54 (dd, ^3J(H,H)=5.9 Hz; ^4J(H,H)=2.6 Hz, 1H), 3.07 ppm (s, 6H); ^{19}F NMR (376 MHz, CD_2Cl_2, 25°C, $CFCl_3$): δ=- 62.81 ppm (s, 3F).

Chloro-2-(3-trifluoromethylphenyl)-4-(*N,N*-dimethylamino)-pyridine mercury (II) (I)

To a *Young Schlenk*, EtOH (25 mL) and AcOH (0.4 mL) were added to a mixture of **A** (400 mg, 1.5 mmol) and $Hg(OAc)_2$ (478 mg, 1.5 mmol). The reaction mixture was then heated at 85°C for 48 h. After 48 h, the reaction mixture was allowed to cool to r.t. Concentrated LiCl in EtOH was added dropwise to the reaction mixture resulting in a colorless precipitate. The precipitate was filtered off and washed with hexane giving the title compound as an off-white solid. The crude product was used without further purification. Yield = 205 mg, 0.41 mmol, 27.3%.

Bis(chloro)-2-(3-trifluoromethylphenyl)-4-(*N,N*-dimethylamino)pyridine gold (III) (a)

To a round bottom flask, **I** (200 mg, 0.4 mmol) dissolved in CH_2Cl_2 and sodium tetrachloroaurate (III) dihydrate (200 mg, 0.5 mmol) dissolved in CH_3CN were added. The reaction mixture was stirred for 24 h at r.t. The colorless precipitate that formed was filtered off and washed with hexane giving the title compound. The product was used without further purification, estimated purity by ^{1}H NMR > 95%. Yield = 195 mg, 0.36 mmol, 61%. ^{1}H NMR (400 MHz, CD_2Cl_2, 25°C, TMS): δ=8.98 (d, ^3J(H,H)=7.5 Hz, 1H), 8.11 (m, 1H), 7.71 (m, 1H), 7.50 (m, 1H), 6.89 (d, ^4J(H,H)=3.1 Hz, 1H), 6.51 (dd, ^3J(H,H)=7.5 Hz; ^4J(H,H)=3.1 Hz, 1H), 3.26 ppm (s, 6H); ^{19}F NMR (376 MHz, CD_2Cl_2, 25 °C, $CFCl_3$): δ=-62.97 ppm (s, 3F).

2-(3-trifluoromethylphenyl)-4-(*N,N*-dimethylamino)pyridine-bis(pentafluorophenyl) gold (III) (1)

In a two-necked round bottom flask, iodopentafluorobenzene (0.03 mL, 0.23 mmol) was added to dry Et_2O (15 mL). To this reaction mixture cooled to –80°C, 1.6 M *n*BuLi (0.14 mL, 0.224 mmol) was added and after 10 min., **a** (50.0 mg, 0.09 mmol) was added. The reaction mixture was allowed to come to r.t. and the residual solvent was removed via N_2-flow. Crude product **1** was purified by flash chromatography on silica (eluent: CH_2Cl_2/hexane 1:1), to afford the pure title compound. Yield = 39.0 mg, 0.055 mmol, 52%. ^{1}H NMR (500 MHz, CD_2Cl_2, 25°C, TMS): δ=7.96 (m, 1H), 7.73 (d, ^3J(H,H)=7.0 Hz, 1H), 7.46 (m, 1H), 7.06 (d, ^4J(H,H)=2.9 Hz, 1H), 6.99 (d, ^3J(H,H)=7.9 Hz, 1H), 6.43 (dd, ^3J(H,H)=7.1 Hz; ^4J(H,H)=2.9 Hz, 1H), 3.22 ppm (s, 6H); ^{13}C NMR (125.78 MHz, CD_2Cl_2, 25°C, TMS): δ=164.1 (s), 161.5 (s), 156.6 (s), 148.8 (s), 147.9–147.6 (m), 147.5 (s), 146.2–145.8 (m), 144.3–144.0 (m), 140.9–140.6 (m), 139.5–138.6 (m), 137.5–137.0 (m), 134.6 (s), 129.8 (q, ^2J(C,C)=32.5 Hz; *C*CF_3), 127.8 (s), 127.4 (q, ^3J(C,C)=3.6 Hz; *C*CCF_3), 126.9–126.1 (m), 124.6 (q, ^1J(C,F)=272.2 Hz; CF_3), 121.3 (s), 121.0 (q, ^3J(C,C)=3.6 Hz; *C*CCF_3), 109.1–108.5 (m), 106.9 (s), 102.3 (s), 40.1 ppm (s; $N(CH_3)_2$); ^{19}F NMR (376 MHz, CD_2Cl_2, 25°C, $CFCl_3$): δ=-62.93 (s, 3F) -121.25 (m, 2F), -121.53 (m, 2F), -158.07 (m, 2F), -158.70 (m, 2F), -161.55 (m, 1F), -162.16 ppm (m, 1F); Elemental analysis (%) calcd for: $C_{26}H_{12}N_2AuF_{13}$: C, 39.22; H, 1.52; N, 3.52; Found: C, 39.22; H, 1.52; N, 3.52.

2-(3-trifluoromethylphenyl)-4-(*N,N*-dimethylamino)pyridine-bis-4-fluorophenyl acetylene (2)

To a flask containing dry Et_2O (10 mL), 1-ethynyl-4-fluorobenzene (0.052 mL, 0.45 mmol) was added and the reaction mixture was cooled to –80°C. To the reaction mixture, 2.5 M *n*BuLi (0.18 mL 0.45mmol) was carefully added leading to a slightly yellowish solution. After stirring the reaction mixture at this temperature for 10 min., **a** (100 mg, 0.188 mmol) was added which led to a color change from yellow to brown. After 1 h, the solvent was removed by a stream of N_2. Crude product **2** was purified by flash chromatography on silica gel (eluent: CH_2Cl_2/hexane 1:1), to afford the pure title compound **2**. Yield = 81.3 mg, 0.116 mmol, 62%. ^{1}H NMR (400 MHz, CD_2Cl_2, 25°C, TMS): δ=9.08 (m, 1H), 8.38 (m, 1H), 7.88 (s, 1H), 7.60 (m, 1H), 7.52 (m, 4H), 7.04 (m, 4H), 6.97 (m, 1H), 6.57 (m, 1H), 3.22 ppm

(s, 6H); ^{13}C NMR (125.78 MHz, CD_2Cl_2, 25°C, TMS): δ=164.2 (s), 163.3 (s), 163.1 (s), 161.3 (s), 161.1 (s), 159.5 (s), 156.4 (s) 149.9 (s), 147.4 (s), 136.3 (s), 133.9–133.7 (m), 129.3 (q, ^2J(C,C)=32.3 Hz, *C*CF_3), 128.5 (s), 127.6–127.5 (m), 127.1 (s), 124.7 (q, ^1J(C,F)=272.2 Hz; CF_3), 122.5–122.4 (m), 120.5 (s), 115.7–155.4 (m), 114.7 (s), 106.7 (s), 102.6 (s), 101.9 (s), 98.1 (s) 40.2 ppm (s; $N(CH_3)_2$); ^{19}F NMR (376 MHz, CD_2Cl_2, 25°C, $CFCl_3$): δ=-62.80 (s, 3F) -113.58 (s, 1F), -113.97 ppm (s, 1F); Elemental analysis (%) calcd for: $C_{30}H_{20}N_2AuF_5$: C, 51.44; H, 2.88; N, 4.00; Found: C, 51.14; H, 2.71; N, 3.85.

2-(4-trifluoromethoxyphenyl)-4-(*N,N*-dimethylamino)pyridine (B)

To a *Schlenk* flask with 2-bromo-4-(*N,N*-dimethylamino)pyridine (802 mg, 3.98 mmol), 4-(trifluoromethoxy)-phenyl)boronic acid (993 mg, 4.82 mmol) and NaOH (386 mg, 9.65 mmol), H_2O (15 mL) and dioxane (25 mL) were added. The brownish reaction mixture was then degassed for 35 min. before $Pd(PPh_3)_4$ dissolved in toluene (10 mL) was added. The reaction mixture was stirred for 97 h at 100°C and was then cooled to r.t. Extraction of the aqueous phase with CH_2Cl_2, drying the combined organic phases over $MgSO_4$ and evaporation of the solvent *in vacuo* delivered the crude product **B**. Crude product **B** was purified by flash chromatography on silica gel (eluent: AcOEt/CH_2Cl_2 2:1), to afford the pure title compound**.** Yield = 301 mg, 1.07 mmol, 27%. ^{1}H NMR (400 MHz, CD_2Cl_2, 25°C, TMS): δ=8.25 (d, ^3J(H,H)=6.0 Hz, 1H), 7.99 (m, 2H), 7.29 (m, 2H), 6.90 (d, ^4J(H,H)=2.6 Hz, 1H), 6.51 (dd, ^4J(H,H)=6.0 Hz; ^3J(H,H)=2.6 Hz, 1H), 3.06 ppm (s, 6H); ^{19}F NMR (376 MHz, CD_2Cl_2, 25°C, $CFCl_3$): δ=-58.15 ppm (s, 3F).

Chloro-2-(4-trifluoromethoxyphenyl)-4-(*N,N*-dimethylamino)pyridine mercury (II) (II)

In a *Young Schlenk* with **c** (300 mg, 1.06 mmol) and $Hg(OAc)_2$ (339 mg, 1.06 mmol), EtOH (25 mL) and 0.4 mL AcOH were added. The reaction mixture was heated at 85°C for 48 h. After, the reaction mixture was allowed to cool to r.t., concentrated LiCl in EtOH was added dropwise. The colorless precipitate that ensued was filtered off and washed with hexane giving crude **II**. The crude product was used further without purification. Yield = 150 mg, 0.29 mmol, 27%. ^{1}H NMR (400 MHz, CD_2Cl_2, 25°C, TMS): δ=8.18 (d, ^3J(H,H)=6.0 Hz, 1H), 8.06 (d, ^4J(H,H)=8.6 Hz, 1H), 7.45 (m, 1H), 7.23 (m, 1H), 7.07 (d, ^4J(H,H)=1.5 Hz, 1 H), 6.60 (m, 1H) 3.10 ppm (s, 6H); ^{19}F NMR (376 MHz, CD_2Cl_2, 25°C, $CFCl_3$): δ=-58.00 ppm (s, 3F).

Bis(chloro)-2-(4-trifluoromethoxyphenyl) 4-(*N,N*-dimethylamino)pyridine gold (III) (b). To a round bottom flask with **III** (150 mg, 0.29 mmol) in CH_2Cl_2, sodium tetrachloroaurate (III) dihydrate (133 mg, 0.33 mmol) dissolved in CH_3CN was added. The reaction mixture was stirred for 24 h at r.t. The colorless precipitate that formed was filtered off and washed with hexane giving **b**. The product was used without further purification, estimated purity by ^{1}H NMR > 95%. Yield = 105 mg, 0.19 mmol, 58%. ^{1}H NMR (400 MHz, CD_2Cl_2, 25°C, TMS): δ=9.05 (m, 1H), 7.92 (m, 1H), 7.62 (m, 1H), 7.26 (m, 1H), 6.83 (m, 1H), 6.52 (m, 1H), 3.23 ppm (s, 6H); ^{19}F NMR (376 MHz, CD_2Cl_2, 25°C, $CFCl_3$): δ=-57.93 ppm (s, 3F).

(2-(4-trifluoromethoxyphenyl))-4-(*N,N*-dimethylamino)pyridine)bis(pentafluorophenyl) gold(III) (3)

To a round bottom flask with dry Et_2O (10 mL), iodopentafluorobenzene (0.05 mL, 0.44 mmol) was added and the reaction mixture was cooled to –80°C. After 5 min., 2.5 M *n*BuLi (0.13 mL, 0.325 mmol) was carefully added to the reaction mixture and a change in color to yellow was observed. After another 5 min., **III** (74.1 mg, 0.14 mmol) was added to the reaction mixture and stirred for 10 min. The solvent was evaporated in *vacuo* and the crude product was purified by flash chromatography on silica gel (eluent: CH_2Cl_2/hexane 1:1), to afford the pure **3**. Yield = 60.3 mg, 0.07 mmol, 53%. ^{1}H NMR (400 MHz, CD_2Cl_2, 25°C, TMS): δ=7.82 (d, ^3J(H,H)=8.6 Hz, 1H), 7.70 (d, ^4J(H,H)=7.0 Hz, 1H), 7.20 (m, 1H), 6.97 (d, ^3J(H,H)=2.9 Hz, 1H), 6.67 (s, 1H), 6.41 (dd, ^4J(H,H)=7.1 Hz; ^3J(H,H)=2.9 Hz, 1H), 3.19 ppm (s, 6H); ^{13}C NMR (100.53 MHz, CD_2Cl_2, 25°C, TMS): δ=164.2 (s), 156.5 (s), 150.7 (s), 148.7 (s), 145.6 (s), 145.2 (s), 125.9 (s), 125.8 (s), 119.5 (s), 106.6 (s), 102.7 (s), 40.0 ppm (s; $N(CH_3)_2$); ^{19}F NMR (376 MHz, CD_2Cl_2, 25°C, $CFCl_3$): δ=-57.98 (s, 3F), -121.23 (m, 2F), -121.57 (m, 2F), -158.09 (m, 2F), -148.45 (m, 2F) -161.57 ppm (m, 1F), -162.16 (m, 1F); Elemental analysis (%) calcd for: $C_{33}H_{11}AuF_{15}N\cdot 1/3C_6H_{14}$: C, 39.99; H, 2.00; N, 3.45; Found: C, 39.82; H, 2.01; N, 2.98.

2-2,3,4-fluorophenyl-4-(*N,N*-dimethylamino)pyridine (C)

To a *Young Schlenk* flask, 2-bromo-4-(*N,N*-dimethylamino)pyridine (1.51 g, 7.51 mmol), (2,3,4-trifluorophenyl)boronic acid (1.59 g, 9.01 mmol) and NaOH pellets (754 mg, 18.9 mmol) were added. To this mixture, H_2O (15 mL) and dioxane (25 mL) were added. After degassing of the reaction mixture, $Pd(PPh_3)_4$ dissolved in toluene (approx. 7 mL), was added. The reaction mixture was then heated to 100°C for 16 h. The reaction mixture was then allowed to cool to room temperature, and the aqueous phase was extracted with CH_2Cl_2. Washing the organic phases with H_2O, drying of the combined organic phases with $MgSO_4$ and evaporation of the solvent *in vacuo* delivered the crude product. The crude product was purified by flash chromatography on silica gel (eluent: CH_2Cl_2/AcOEt 1:2) to afford the title compound. Yield = 244 mg, 0.97 mmol, 13%. ^{1}H NMR (400 MHz, CD_2Cl_2, 25°C, TMS): δ=8.27 (d, ^3J(H,H)=6.0 Hz, 1H), 7.52 (m, 1H), 7.08 (m, 1H), 6.93 (m, 1H), 6.52 (dd, ^3J(H,H)=6.0 Hz; ^4J(H,H)=2.6 Hz, 1H), 3.04 ppm (s, 6H); ^{19}F NMR (376 MHz, CD_2Cl_2, 25°C, $CFCl_3$): δ=-135.97 (m, 1F), -139.07 (m, 1F), -162.20 ppm (m, 1F).

Chloro-(2-2,3,4-fluorophenyl-4-(*N,N*-dimethylamino)pyridine) mercury (II) (III)

To a *Young Schlenk* with **C** (320 mg, 1.27 mmol) and $Hg(OAc)_2$ (403 mg, 1.27 mmol), EtOH (25 mL) and 0.4 mL AcOH were added. The reaction mixture was heated at 85°C for 48 h. After the reaction mixture was allowed to cool to r.t., concentrated LiCl solution in EtOH was added dropwise to the reaction mixture. The formed colorless precipitate was filtered off and washed

with hexane to crude pure **III**. The crude product was used without further purification. Yield = 276 mg, 0.57 mmol, 45%.

Bis(chloro)-2-2,3,4-fluorophenyl-4-(*N,N*-dimethylamino)pyridine gold (III) (c)

To a round bottom flask, **III** (276 mg, 0.57 mmol) dissolved in CH_2Cl_2 and sodium tetrachloroaurate (III) dihydrate (258 mg, 0.65 mmol) dissolved in CH_3CN were added. The reaction mixture was stirred for 24 h at r.t. The formed colorless precipitate was filtered off and washed with hexane to give **c**. The product was used without further purification, estimated purity by ^{1}H NMR > 95%. Yield = 181 mg, 0.35 mmol, 54%. ^{1}H NMR (400 Hz, CD_2Cl_2, 25°C, TMS): δ=9.07 (d, ^3J(H,H) =7.5 Hz, 1H), 7.82 (m, 1H), 7.24 (m, 1H), 6.54 (m, 1H), 3.22 ppm (s, 6H); ^{19}F NMR (376 MHz, CD_2Cl_2, 25°C, $CFCl_3$): δ=-128.43 (m, 1F), -134.51 (m, 1F), -160.34 ppm (m, 1F).

2-2,3,4-fluorophenyl-4-(*N,N*-dimethylamino)pyridine-bis(pentafluorophenyl) gold (III) (4)

To a two-necked round bottom flask with dry Et_2O (15 mL), iodopentafluorobenzene (0.05 mL, 0.37 mmol) was added. The reaction mixture was cooled to –80°C and 2.5 M *n*BuLi (0.09 mL, 0.225 mmol) was added. After 10 min. of stirring, **c** (47.0 mg, 0.09 mmol) was added and a change in color to a greenish solution was observed which further turned to a colorless solution. The reaction was allowed to stir for 30 min. and after the solvent was removed via N_2-flow resulting in a crude product. This was further purified by flash chromatography on silica gel (eluent: CH_2Cl_2/hexane 1:1), to afford pure **4.** Yield = 27.3 mg, 0.035 mmol, 39%. ^{1}H NMR (400 MHz, CD_2Cl_2, 25°C, TMS): δ=7.69 (d, ^3J(H,H)=7.0 Hz, 1H), 7.44 (m, 1H), 6.47 (m, 1H), 6.39 (dd, ^3J(H,H)=7.0 Hz; ^4J(H,H)=2.6 Hz, 1H), 3.18 ppm (s, 6H); ^{13}C NMR (125.78 MHz, CD_2Cl_2, 25°C, TMS): δ=161.8–161.7 (m), 156.6 (s), 152.9–152.8 (m), 151.9 (s), 151.1–151.0 (m), 150.9–150.8 (m), 149.0–148.9 (m), 148.8 (s), 147.8–147.6 (m), 146.1–145.7 (m), 144.2–144.0 (m), 141.0–140.7 (m), 140.0–138.7 (m), 137.5–137.0 (m), 131.1 (s), 125.6–124.6 (m), 117.4–117.3 (m), 108.9–108.3 (m), 106.1 (s), 106.0 (s), 34.0 ppm (s; $N(CH_3)_2$); ^{19}F NMR (376 MHz, CD_2Cl_2, 25°C, $CFCl_3$): δ=-121.40 (m, 1F), -131.04 (m, 1F), -135.37 (m,1F), -157.73 (t, 2F), -158.09 (t, 2F), -161.39 (m, 2F), -161.73 (m, 2F), -162.35 ppm (m, 2F); Elemental analysis (%) calcd for: $C_{25}H_{11}N_2AuF_{13}$: C, 38.38; H, 1.29; N, 3.58; Found: C, 38.20; H, 1.23; N, 3.51.

Computational details

The *Gaussian 09* program package[14] was used for all density functional theory (DFT) and time-dependent DFT (TD-DFT) calculations reported in the manuscript. The properties of compounds **1, 2, 3** and **4** were studied using the hybrid functional PBE1PBE[15] associated with the Stuttgart/Dresden effective core potentials (SDD) basis set[16] for the Au center augmented with one *f*-polarization function (α = 1.050), with the standard 6-31+G(d) basis set[17] for the remaining atoms, and with the conductive polarizable continuum model (CPCM)[18] to take the solvent effects into acount (dichloromethane). The molecular structures of the ground states and lowest triplet states were obtained by restricted calculations for the ground states and unrestricted calculations for the the triplet states without symmetry restriction. The final geometries were confirmed to be potential energy minima by vibrational frequency calculations at the same level of theory, as no imaginary frequency was found. On the DFT optimized ground-state S_0 geometries, TD-DFT calculations[19] were used to produce the first 25 lowest singlet–singlet and the first 3 singlet–triplet vertical excitations with the corresponding energies, transition coefficients and oscillator strengths. The singly occupied molecular orbitals were obtained by restricted open-shell single point calculations on the optimized triplet state geometries. The frontier orbital surfaces and spin density distributions reported herein were generated by *Gaussview*[20] on *Gaussian 09* formatted checkpoint output files with isovalues set to 0.02 and 0.004, respectively. The alkyne-containing compound **2** was further investigated as we noticed that the character of the first triplet excited state T_1 varies with the rotation of the terminal fluorobenzene ligands. The fully optimized structure of **2** was called **2A** and corresponds to an almost planar molecule. The conformation with the fluorobenzene rings frozen perpendicular to the cyclometalated ligand is denoted **2B**. Several "in-between" conformations characterized by fixed dihedral angle values of 15, 30, 45, 60 and 75° were also investigated.

X-ray crystallography

The single-crystal X-ray diffraction data was collected at 183(1) K on an *Agilent Technologies Xcalibur Ruby* area-detector diffractometer using a single wavelength Enhance X-ray source with Mo K_a radiation (l = 0.71073 Å)[21] from a micro-focus X-ray source and an *Oxford Instruments Cryojet XL* cooler. The selected suitable single crystal was mounted using polybutene oil on a flexible loop fixed on a goniometer head and immediately transferred to the diffractometer. The pre-experiment, data collection, data reduction and analytical absorption correction[22] were performed with the program suite *CrysAlisPro*.[23] Using *Olex2*,[24] the structure was solved with the SHELXT[25] small molecule structure solution program and refined with the *SHELXL2014*[26] program package by full-matrix least-squares minimization on F^2. *PLATON*[27] was used to check the result of the X-ray analysis. For more details about the data collection and refinements parameters, see the Supporting Information and the Crystallographic Information file. CCDC-1511251 (complex **4**) contains the supplementary crystallographic data for this paper. The data can be obtained free of charge from The Cambridge Crystallographic Data Centre via www.ccdc.cam.ac.uk/data_request/cif.

Acknowledgements

The authors wish to thank Prof. Roger Alberto for the generous support. Financial support from the Swiss National Science Foundation (Grant no. 200020_156967) and the University of Zurich is gratefully acknowledged.

Keywords: Gold • Phosphorescence • Blue • Fluorine • Cyclometalated

[1] a) P.-T. Chou, Y. Chi, M.-W. Chung and C.-C. Lin, *Coord. Chem. Rev.* **2011**, *255*, 2653-2665; b) P. T. Chou and Y. Chi, *Eur. J. Chem.* **2007**, *13*, 380-395; c) M. A. Baldo, D. F. O'Brien, Y. You, A. Shoustikov, S. Sibley, M. E. Thompson and S. R. Forrest, *Nature* **1998**, *395*, 151-154; d) S. Kappaun, C. Slugovc and E. J. W. List, *Int. J. Mol. Sci.* **2008**, *9*, 1527-1547; e) M. K. Nazeeruddin and M. Grätzel, *Structure and Bonding* 2007, *123*, 113-175; f) R. Visbal, J. M. Lopez-de-Luzuriaga, A. Laguna and M. C. Gimeno, *Dalton Trans.* **2014**, *43*, 328-334; g) M. Bardají, A. Laguna, V. M. Orera and M. D. Villacampa, *Inorg. Chem.* **1998**, *37*, 5125-5130; h) L. Huang, M. Rudolph, F. Rominger and A. S. K. Hashmi, *Angew. Chem. Int. Ed.* **2016**, *55*, 4808-4813; i) L. Huang, F. Rominger, M. Rudolph and A. S. K. Hashmi, *Chem. Commun.* **2016**, *52*, 6435-6438.

[2] a) K. M.-C. Wong, L.-L. Hung, W. H. Lam, N. Zhu and V. W.-W. Yam, *J. Am. Chem. Soc.* **2007**, *129*, 11662-11662; b) C.-W. Chan, W.-T. Wong and C.-M. Che, *Inorg. Chem.* **1994**, *33*, 1266-1272.

[3] a) L. Gao, D. V. Partyka, J. B. Updegraff, N. Deligonul and T. G. Gray, *Eur. J. Inorg. Chem.* **2009**, *2009*, 2711-2719; b) M. Vijayakumar and M. S. Gopinathan, *J. Mol. Struct.: THEOCHEM.* **1996**, *361*, 15-19.

[4] a) W.-P. To, K. T. Chan, G. S. M. Tong, C. Ma, W.-M. Kwok, X. Guan, K.-H. Low and C.-M. Che, *Angew. Chem. Int. Ed.* **2013**, *52*, 6648-6652; b) W.-P. To, G. S.-M. Tong, W. Lu, C. Ma, J. Liu, A. L.-F. Chow and C.-M. Che, *Angew. Chem. Int. Ed.* **2012**, *51*, 2654-2657; c) J. J. Yan, A. L.-F. Chow, C.-H. Leung, R. W.-Y. Sun, D.-L. Ma and C.-M. Che, *Chem. Commun.* **2010**, *46*, 3893-3895.

[5] a) V. W.-W. Yam, S. W.-K. Choi, T.-F. Lai and W.-K. Lee, *J. Chem. Soc., Dalton Trans.* **1993**, 1001-1002; b) V. W.-W. Yam, T.-F. Lai and C.-M. Che, *J. Chem. Soc., Dalton Trans.* **1990**, 3747-3752.

[6] a) V. K.-M. Au, K. M.-C. Wong, N. Zhu and V. W.-W. Yam, *J. Am. Chem. Soc.* **2009**, *131*, 9076-9085; b) K. M.-C. Wong, X. Zhu, L.-L. Hung, N. Zhu, V. W.-W. Yam and H.-S. Kwok, *Chem. Commun.* **2005**, 2906-2908; c) V. K.-M. Au, K. M.-C. Wong, N. Zhu and V. W.-W. Yam, *Eur. J. Chem.* **2011**, *17*, 130-142; d) V. W.-W. Yam and E. C.-C. Cheng, *Chem. Soc. Rev.* **2008**, *37*, 1806-1813; e) V. K.-M. Au, K. M.-C. Wong, D. P.-K. Tsang, M.-Y. Chan, N. Zhu and V. W.-W. Yam, *J. Am. Chem. Soc.* **2010**, *132*, 14273-14278; f) V. K.-M. Au, W. H. Lam, W.-T. Wong and V. W.-W. Yam, *Inorg. Chem.* **2012**, *51*, 7537-7545.

[7] a) A. Herbst, C. Bronner, P. Dechambenoit and O. S. Wenger, *Organometallics* **2013**, *32*, 1807-1814; b) P. I. da S. Maia, H. H. Nguyen, D. Ponader, A. Hagenbach, S. Bergemann, R. Gust, V. M. Deflon and U. Abram, *Inorg. Chem.* **2012**, *51*, 1604-1613; c) C. Nevado and R. Kumar, *Angew. Chem. Int. Ed.* **2016**, **DOI:** 10.1002/anie.201607225; d) J. Fernandez-Cestau, B. Bertrand, M. Blaya, G. A. Jones, T. J. Penfold and M. Bochmann, *Chem. Commun.* **2015**, *51*, 16629-16632.

[8] a) J. A. Garg, O. Blacque, T. Fox and K. Venkatesan, *Inorg. Chem.* **2010**, *49*, 11463-11472; b) J. A. Garg, O. Blacque and K. Venkatesan, *Inorg. Chem.* **2011**, *50*, 5430-5441; c) A. Szentkuti, M. Bachmann, J. A. Garg, O. Blacque and K. Venkatesan, *Eur. J. Chem.* **2014**, *20*, 2585-2596; d) M. Bachmann, O. Blacque and K. Venkatesan, *Dalton Trans.* **2015**, *44*, 10003-10013; e) A. Szentkuti, J. A. Garg, O. Blacque and K. Venkatesan, *Inorg. Chem.* **2015**, *54*, 10748-10760.

[9] a) Y. L. Chang and Z. H. Lu, *J. Disp. Technol.* **2013**, *9*, 459-468; b) H. Fu, Y.-M. Cheng, P.-T. Chou and Y. Chi, *Mater. Today* **2011**, *14*, 472-479; c) G. Zhou, W.-Y. Wong and S. Suo, *J. Photochem. Photobiol., C* **2010**, *11*, 133-156; d) L. Xiao, Z. Chen, B. Qu, J. Luo, S. Kong, Q. Gong and J. Kido, *Adv. Mater.* **2011**, *23*, 926-952; e) H. Sasabe and J. Kido, *J. Mater. Chem. C* **2013**, *1*, 1699-1707; f) K. S. Yook and J. Y. Lee, *Adv. Mater.* **2012**, *24*, 3169-3190; g) C. L. Mulder, K. Celebi, K. M. Milaninia and M. A. Baldo, *Appl. Phys. Lett.* **2007**, *90*, 211109; h) J. Lee, H.-F. Chen, T. Batagoda, C. Coburn, P. I. Djurovich, M. E. Thompson and S. R. Forrest, *Nat Mater* **2016**, *15*, 92-98.

[10] A. J. Lees, *Chem. Rev.* **1987**, *87*, 711-743.

[11] a) D.-A. Rosca, D. A. Smith and M. Bochmann, *Chem. Commun.* **2012**, *48*, 7247-7249; b) A. S. K. Hashmi, C. Lothschütz, M. Ackermann, R. Doepp, S. Anantharaman, B. Marchetti, H. Bertagnolli and F. Rominger, *Eur. J. Chem.* **2010**, *16*, 8012-8019.

[12] a) Q.-L. Xu, C.-C. Wang, T.-Y. Li, M.-Y. Teng, S. Zhang, Y.-M. Jing, X. Yang, W.-N. Li, C. Lin, Y.-X. Zheng, J.-L. Zuo and X.-Z. You, *Inorg. Chem.* **2013**, *52*, 4916-4925; b) R. Uson, A. Laguna and J. Vicente, *J. Organomet. Chem.* **1977**, *131*, 471-475; c) R. Usón, J. Vicente, J. A. Cirac and M. T. Chicote, *J. Organomet. Chem.* **1980**, *198*, 105-112.

[13] E. Baranoff and B. F. E. Curchod, *Dalton Trans.* **2015**, *44*, 8318-8329.

[14] G. W. T. M. J. Frisch, H. B. Schlegel, G. E. Scuseria, M. A. Robb, J. R. Cheeseman, G. Scalmani, V. Barone, B. Mennucci, G. A. Petersson, H. Nakatsuji, M. Caricato, X. Li, H. P. Hratchian, A. F. Izmaylov, J. Bloino, G. Zheng, J. L. Sonnenberg, M. Hada, M. Ehara, K. Toyota, R. Fukuda, J. Hasegawa, M. Ishida, T. Nakajima, Y. Honda, O. Kitao, H. Nakai, T. Vreven, J. A. Montgomery, Jr., J. E. Peralta, F. Ogliaro, M. Bearpark, J. J. Heyd, E. Brothers, K. N. Kudin, V. N. Staroverov, T. Keith, R. Kobayashi, J. Normand, K. Raghavachari, A. Rendell, J. C. Burant, S. S. Iyengar, J. Tomasi, M. Cossi, N. Rega, J. M. Millam, M. Klene, J. E. Knox, J. B. Cross, V. Bakken, C. Adamo, J. Jaramillo, R. Gomperts, R. E. Stratmann, O. Yazyev, A. J. Austin, R. Cammi, C. Pomelli, J. W. Ochterski, R. L. Martin, K. Morokuma, V. G. Zakrzewski, G. A. Voth, P. Salvador, J. J. Dannenberg, S. Dapprich, A. D. Daniels, O. Farkas, J. B. Foresman, J. V. Ortiz, J. Cioslowski, and D. J. Fox. in *Gaussian 09*, *Vol.* Gaussian, ing., Wallingford CT, **2013**, p. Gaussian 09.

[15] C. Adamo and V. Barone, *J. Chem. Phys.* **1999**, *110*, 6158-6170.

[16] T. H. H. Jr Dunning, P.; Plenum: New York, , *Mod. Theor. Chem.* **1976**, *3*.

[17] R. Ditchfield, W. J. Hehre and J. A. Pople, *J. Chem. Phys.* **1971**, *54*, 724-728.

[18] a) V. Barone and M. Cossi, *J. Phys. Chem. A* **1998**, *102*, 1995-2001; b) M. R. Cossi, N.; Scalmani, G.; Barone, V. , *J. Comput. Chem.* **2003**, *24*, 669.

[19] a) R. Bauernschmitt and R. Ahlrichs, *Chem. Phys. Lett.* **1996**, *256*, 454-464; b) M. E. Casida, C. Jamorski, K. C. Casida and D. R. Salahub, *J. Chem. Phys.* **1998**, *108*, 4439-4449; c) R. E. Stratmann, G. E. Scuseria and M. J. Frisch, *J. Chem. Phys.* **1998**, *109*, 8218-8224.

[20] V. GaussView, Dennington, R.; Keith, T.; Millam, J. Semichem Inc., Shawnee Mission, KS, 2009.

[21] T. Rigaku Oxford Diffraction (formerly Agilent Technologies). Rigaku Corporation, Japan.

[22] R. C. Clark and J. S. Reid, *Acta Crystallogr., Sect. A* **1995**, *51*, 887-897.

[23] V. R. C. Rigaku Oxford Diffraction. CrysAlisPro, Tokyo, Japan.

[24] O. V. Dolomanov, L. J. Bourhis, R. J. Gildea, J. A. K. Howard and H. Puschmann, *J. Appl. Crystallogr.* **2009**, *42*, 339-341.

[25] G. Sheldrick, *Acta Crystallogr., Sect. A* **2015**, *71*, 3-8.

[26] G. Sheldrick, *Acta Crystallogr., Sect. C* **2015**, *71*, 3-8.

[27] A. Spek, *Acta Crystallogr., Sect. D* **2009**, *65*, 148-155.

10.1002/chem.201605567

WILEY-VCH

FULL PAPER

Blue emitting gold(III) complexes were achieved through rational modifications of the phenylpyridine ligand scaffold.

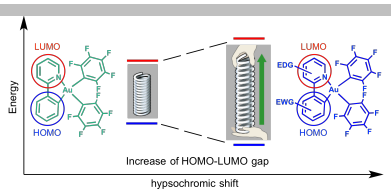

Michael Bachmann, Jasmin Terreni, Olivier Blacque, and Koushik Venkatesan[a]*

Page No. – Page No.

Rationally Designed Blue Triplet Emitting Gold(III) Complexes Based on Phenylpyridine Derived Framework